A New Watermarking Method Based on the Use of the Hyperanalytic Wavelet Transform

Corina Nafornita[a], Ioana Firoiu[a], Jean-Marc Boucher[b], Alexandru Isar[a*]

[a]Electronics and Communications Faculty, Politehnica University, B-dul V. Parvan 2, Timisoara, Romania, {corina.nafornita, ioana.firoiu, alexandru.isar}@etc.upt.ro

[b] GET/ENST Bretagne, TAMCIC/CNRS UMR 2872, Technopole Brest-Iroise, CS 83818-29238 Brest Cedex 3
France, email : jm.boucher@enst-bretagne.fr

ABSTRACT

Watermarking using pixel-wise masking in the wavelet domain proves to be quite robust against common signal processing attacks. Initially, in a system proposed by Barni *et al.*, embedding is made only in the highest resolution level; there are two disadvantages to this technique: the watermark information can be easily erased by a potential attacker and embedding in the DWT is susceptible to geometric attacks, such as shifting. To enhance this watermarking method, we use a modified perceptual mask that models the human visual system behavior in a better way, previously proposed by the authors. The texture content is appreciated with the local standard deviation of the original image, which is further compressed in the wavelet domain. Since the approximation image of the coarsest level contains too little information, we appreciate the luminance content using a higher resolution level approximation sub-image. To increase the capacity of the watermarking scheme the embedding is made in the HWT domain, using two strategies: in the real parts of the HWT coefficients and in the absolute value of the HWT coefficients of the original image. The implementation of the HWT is made using a new technique, recently proposed by the authors. Moreover, we make use of all the levels except the coarsest one, for attack resilience. We use three types of detectors that take advantage of the hierarchical decomposition. Tests were made for different attacks (JPEG compression, median filtering, resizing, cropping, gamma correction, blurring, shifting and addition of white Gaussian noise), that prove the effectiveness of perceptual watermarking in the HWT domain.

Keywords: Pixel-wise mask, robust watermark, wavelets, hyper analytic wavelet transform.

1. INTRODUCTION

Digital watermarks have recently emerged as a means to protect the copyright of digital images. The majority of watermarking algorithms operate based on the spread spectrum communication principle. A pseudorandom sequence is added to the host image in some critically sampled domain and the watermarked image is obtained by inverse transforming the modified image coefficients. The Discrete Wavelet Transform (DWT), the (block-based) Discrete Cosine Transform (DCT) and the Discrete Fourier Transform (DFT) are some of the most popular transform domains. Numerous Wavelet Transforms (WTs) can be used to embed the watermark. The first one was the DWT, [1]. The DWT based algorithms usually produce watermarked images with the best balance between visual quality and robustness due to the absence of blocking artifacts. It has three main disadvantages, [2]: lack of shift invariance, lack of symmetry of the mother wavelets and poor directional selectivity. Caused by the lack of shift invariance of the DWT, small shifts in the input signal can produce important changes in the energy distribution of the wavelet coefficients. Due to the poor directional selectivity for diagonal features of the DWT the watermarking capacity is small. The most important parameters of a watermarking system are robustness against attacks and capacity. These parameters must be maximized. These disadvantages can be diminished using a complex wavelet transform [2, 3]. Over twenty years ago, Grossman and Morlet [4] developed the Continuous Wavelet Transform (CWT) [5], using continuous complex-valued mother wavelets. Initial analysis based on wavelet decompositions was implemented using such mother wavelets. Both magnitude and

phase descriptions of non-stationary signals were determined, and an early example of analysis includes wavelet ridge methods proposed by Delprat *et al.* [6]. However subsequently for many years interest focused on the DWT. The DWT was developed to implement the WT of time-compact mother wavelets and as compact discrete wavelet filters cannot be exactly analytic [7], real wavelets were used. A revival of interest in later years has occurred in both signal processing and statistics for the usage of complex wavelets, [8], and in particular complex analytic wavelets [9]–[11]. This revival of interest may be linked to the development of complex-valued discrete wavelet filters [12] and the clever dual filter bank [9, 5]. The complex wavelet transform has been shown to provide a powerful tool in signal and image analysis [13], where most of the properties of the transform follow from the analyticity of the wavelet function. Large classes of wavelets were derived in [14], generalizing the concept of a 1-D local complex-valued analytic decomposition to a 2-D vector-valued hyperanalytic decomposition. In the present paper we propose the use of a very simple implementation of the Hyperanalytic Wavelet Transform, (HWT), recently proposed, [15]. It has a high shift-invariance degree versus other quasi-shift-invariant WTs at same redundancy. It has also an enhanced directional selectivity. All the WTs have two parameters: the mother wavelets, (MW) and the primary resolution, (PR), (number of iterations). The importance of their selection is highlighted in [16]. Another appealing particularity of those transforms, coming from their multiresolution capability, is the interscale dependency of the wavelet coefficients. This paper proposes an application of the new implementation of HWT, already mentioned [15]. The second paragraph describes this implementation. The third paragraph is dedicated to the proposed watermarking method. Some simulation results are reported in the fourth paragraph and the paper's conclusion is formulated in the last paragraph.

2. A NEW IMPLEMENTATION OF HWT

A 1D WT is shift-sensitive if an input signal shift causes an unpredictable change of the transform coefficients. The shift-sensitivity of the DWT is generated by the down-samplers used for its computation. In [13, 17] is devised the un-decimated DWT (UDWT), which is a WT without down-samplers. It has high redundancy, 2^J (where J represents the number of iterations of the WT) and it requires the implementation of a large number of different filters. In [18] was proposed a new shift-invariant but very redundant WT, named Shift Invariant Discrete Wavelet Transform, (SIDWT). The corresponding algorithm is called Cycle Spinning (CS) and can be equivalent to SIDWT. In [19], is demonstrated that approximate shiftability is possible for the DWT with a small, fixed amount of transform redundancy. In this reference is designed a pair of real mother wavelets such that one is approximately the Hilbert transform of the other. In the following we will give the mathematical bases for this approach. In [20] the author has given a way to built new complete orthonormal sets of the Hilbert space of finite energy band-limited functions with bandwidth π, named the Paley-Wiener space, (PW). Following the proposition proved in [20] some new orthonormal complete sets of integer translates of a generating function can be constructed for the space PW. The scaling function and the mother wavelets of the standard multi-resolution analysis of PW generate by integers translate such complete orthonormal sets. The proposition proved in [20] was generalized in [21] to give a new mechanism of mother wavelets construction. In this last reference were formulated two new propositions. These two propositions can be used to construct new mother wavelets.

For example if the function ψ is a mother wavelets then the functions $j\mathcal{H}\{\psi\}$ and $\psi_a = \psi + j\mathcal{H}\{\psi\}$ are also mother wavelets. This wavelet pair $(\psi, j\mathcal{H}\{\psi\})$ defines a complex discrete wavelet transform (CDWT) presented in figure 1 a). A complex wavelet coefficient is obtained by interpreting the wavelet coefficient from one DWT tree as being its real part, whereas the corresponding coefficient from the other tree is interpreted as its imaginary part. In [2] is developed the dual tree complex wavelet transform (DT-CWT), which is a quadrature pair of DWT trees, similar to the CDWT. The DT-CWT coefficients may be interpreted as arising from the DWT associated with a quasi-analytic wavelet. Both DT-CWT and CDWT are invertible and quasi shift-invariant; however the design of these quadrature wavelet pairs is quite complicated and it can only be done through approximations. The implementation of the HWT representing the aim of our proposal is presented in figure 1 b). We first apply a Hilbert transform to the data. The real wavelet transform is then applied to the analytical signal associated to the input data, obtaining complex coefficients. The two implementations of the CDWT presented in figure 1 are equivalent because:

$$\begin{aligned} d_{DTCWT}[m,n] &= \left\langle x(t), \psi_{m,n}(t) + i\mathcal{H}\left\{\psi_{m,n}(t)\right\}\right\rangle = \left\langle x(t), \psi_{m,n}(t)\right\rangle - i\left\langle x(t), \mathcal{H}\left\{\psi_{m,n}(t)\right\}\right\rangle = \\ &= \left\langle x(t), \psi_{m,n}(t)\right\rangle + i\left\langle \mathcal{H}\{x(t)\}, \psi_{m,n}(t)\right\rangle = \left\langle x(t) + i\mathcal{H}\{x(t)\}, \psi_{m,n}(t)\right\rangle = d_{HWT}[m,n] \end{aligned} \tag{1}$$

In fact neither the DT CWT nor the proposed implementation of HWT correspond to perfect analytic mother wavelets, because the exact digital implementation of a Hilbert transform pair of mother wavelets with good performance is not

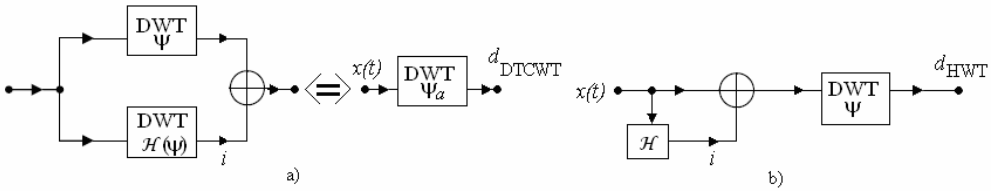

Fig. 1. The implementation of the DT CWT a) and of the HWT b) are equivalent

possible in the case of the first transform and because the digital Hilbert transformer is not a realizable system in the case of the second transform. The DT-CWT requires special mother wavelets (the implementation of the HWT proposed in figure 1 b) can be realized using classical mother wavelets like those conceived by Daubechies) but can assure a higher degree of shift invariance. These two transforms have in the 1D case a redundancy of 2. In [22] is proposed a two-stage mapping-based complex wavelet transform (MBCWT) that consists of a mapping onto a complex function space followed by a DWT of the complex mapping computation. The authors of this article have observed that the DT CWT coefficients admit also another interpretation: they may be interpreted as the coefficients of a DWT applied to a complex signal associated with the input signal. The complex signal is defined as the Hardy-space image of the input signal. As the Hardy-space mapping of a discrete signal is impossible to compute, they have defined a new function space called the Softy-space, which is an approximation to Hardy-space. The HWT implementation presented in figure 1 b) can be regarded like a MBCWT where the mapping system is a Hilbert transformer. The advantages of the MBCWT are:

- controllable redundancy of the mapping stage (there are non-redundant implementations of this transform);

- the possibility to use any mother wavelets, which provides flexibility to this transform (the proposed implementation of the HWT has also this advantage).

The generalization of the analyticity concept in 2D is not obvious, because there are multiple definitions of the Hilbert transform in this case. In the following we will use the definition of the analytic signal associated to a 2D real signal named hyper-complex signal. So, the hyper-complex mother wavelet associated to the real mother wavelet $\psi(x,y)$ is defined as:

$$\psi_a(x,y) = \psi(x,y) + i\mathcal{H}_x\{\psi(x,y)\} + j\mathcal{H}_y\{\psi(x,y)\} + k\mathcal{H}_x\{\mathcal{H}_y\{\psi(x,y)\}\} \tag{3}$$

where $i^2 = j^2 = -k^2 = -1,$ and $ij = ji = k$, [24]. The HWT of the image $f(x,y)$ is:

$$HWT\{f(x,y)\} = \langle f(x,y), \psi_a(x,y)\rangle. \tag{4}$$

Taking into account relation (3) it can be written:

$$\begin{aligned} &HWT\{f(x,y)\} = DWT\{f(x,y)\} + iDWT\{\mathcal{H}_x\{f(x,y)\}\} + \\ &+ jDWT\{\mathcal{H}_y\{f(x,y)\}\} + kDWT\{\mathcal{H}_y\{\mathcal{H}_x\{f(x,y)\}\}\} = \langle f_a(x,y), \psi(x,y)\rangle = DWT\{f_a(x,y)\}. \end{aligned} \tag{5}$$

The 2D-HWT of the image $f(x,y)$ can be computed with the aid of the 2D-DWT of its associated hyper-complex image. The new HWT implementation, [15, 25] (figure 2), uses four trees, each one implementing a 2D-DWT. A comparison of the directional selectivity of the 2D-DWT and the proposed 2D-HWT is presented in figure 3. The first tree is applied to the input image. The second and the third trees are applied to 1D discrete Hilbert transforms computed across the lines ($\mathcal{H}_x$) or columns ($\mathcal{H}_y$) of the input image. The fourth tree is applied to the result obtained after the computation of the two 1D discrete Hilbert transforms of the input image. The enhancement of the directional selectivity of the 2D-HWT is realized as in the case of the 2D-DTCWT, [3, 5], by linear combinations of detail coefficients belonging to each sub-band of each of the four 2D-DWTs. We have conceived a special input image, in the frequency domain, to conduct this simulation. Its spectrum, represented in figure 3, is oriented following the directions: 0, ±atan(1/2), ±π/4, 0, ±atan(2) and π. The better directional selectivity of the new implementation of 2D-HWT versus the 2D-DWT can be easily observed. For example, this new implementation makes the difference between the two principal diagonals or between the directions ±atan(1/2) whereas the DWT cannot make such differences.

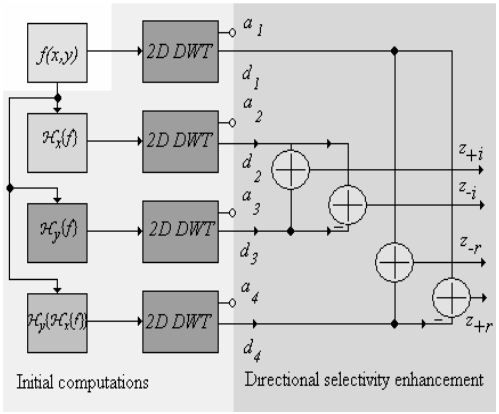

Fig. 2. The new 2D-HWT-implementation architecture.

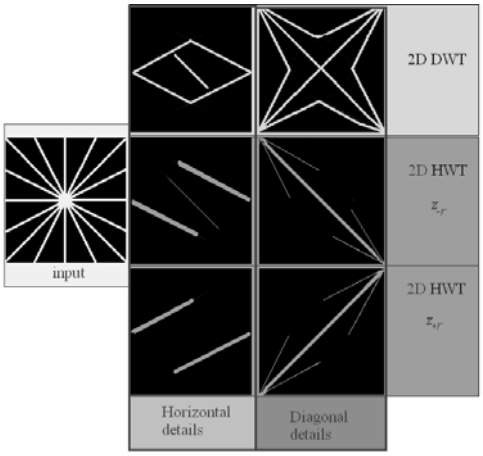

Fig. 3. The absolute values of the spectra of horizontal and diagonal detail sub-images obtained after the first iterations of 2D DWT and 2D HWT (proposed implementation).

3. WATERMARKING BASED ON THE NEW IMPLEMENTATION OF THE HWT

The watermark capacity was studied in [26] where an information-theoretic model for image watermarking and data hiding is presented. Models for geometric attacks and distortion measures that are invariant to such attacks are also considered. The lack of shift invariance of the DWT and its poor directional selectivity are reasons to embed the watermark in the field of another WT. To maximize the robustness and the capacity, the role of the redundancy of the transform used must be highlighted first. An example of redundant WT is represented by the tight frame decomposition. In [27] are analyzed the watermarking systems based on tight frame decompositions. The analysis indicates that a tight frame offers no inherent performance advantage over an orthonormal transform (DWT) in the watermark detection process despite the well known ability of redundant transforms to accommodate greater amounts of added noise for a given distortion. The overcompleteness of the expansion, which aids the watermark insertion by accommodating greater watermark energy for a given distortion, actually hinders the correlation operator in watermark detection. As a result, the tight-frame expansion does not inherently offer greater spread-spectrum watermarking performance. This analytical observation should be tempered with the fact that spread-spectrum watermarking is often deployed in conjunction with an image-adaptive weighting mask to take into account the human visual model (HVM) and to improve perceptual performance. Another redundant WT, the DT-CWT, was already used for watermarking, [28]. The authors of this paper prove that the capacity of a watermarking system based on a complex wavelet transform is higher than the capacity of a similar system that embeds the watermark in the DWT domain. Many authors (e.g. Daugman [29]) have suggested that the processing of visual data inside our visual cortex resembles filtering by an array of Gabor filters of different orientations and scales. We have already proved that the proposed implementation of HWT is efficient, has only a modest amount of redundancy, provides approximate shift invariance, has better directional selectivity than the 2D DWT and it can be observed that the corresponding basis functions closely approximate the Gabor functions. So, the spread spectrum watermarking based on the use of an image adaptive weighting mask applied in the 2D-HWT domain is potentially a robust solution that increases the capacity. The aim of this paper is to present two new perceptual watermarking techniques in the HWT domain. In the first case, we embed the watermark in the images z_{+r} and z_{-r}, using a perceptual mask; while the blind detection is made on the couple (z_{+r}, z_{-r}). A second approach embeds the watermark in the absolute values of the HWT. The two approaches are compared with the classical approach in the DWT domain, from Barni's method [30] and the method proposed in [31].

3.1 Perceptual watermarks embedded in the DWT domain

One of the qualities required to a watermark is its imperceptibility. There are some ways to assure this quality. One way is to embed the watermark in coefficients of known robustness (which are usually large coefficients) or perceptually significant regions, i.e. contours and textures of an image. This can be done empirically, selecting larger coefficients or

using a thresholding scheme in the transform domain [33, 34]. Another approach is to insert the watermark in all coefficients of a transform, using a variable strength for each coefficient [30, 31]. Hybrid techniques, based on compression schemes, embed the watermark using a thresholding scheme and variable strength [33]. Specifically we will only refer to the techniques presented in [30] and [31]. The watermark is masked according to the characteristics of the human visual system (HVS), taking into account the texture and the luminance content of all the image subbands [30, 31]. For coefficients corresponding to contours of the image a higher strength is used, for textures a medium strength is used and for regions with high regularity a lower strength is used, in accordance with the analogy water-filling and watermarking proposed by Kundur in [32]. Barni's method [30] is quite robust against common signal processing attacks like filtering, compression, cropping etc. However, because embedding is made only in the highest resolution level, the watermark information can be easily erased by a potential attacker. In [31], a new pixel-wise mask was used in the DWT domain that models the HVS behavior in a better way thus allowing embedding of the watermark in all resolution levels, except the last one. At the detection, since the threshold is image dependent, the ratio between correlation and threshold was used; hence the detection function becomes nonlinear with a fixed detection threshold. Three types of detectors are being used, to take advantage of the wavelet hierarchical decomposition. The watermark presence is detected 1) from all resolution levels, 2) separately, considering the maximum detector response from each level and 3) separately, considering the maximum detector response from each subband. Evaluating correlations separately per resolution level or subband is sometimes advantageous. For cropping, the watermark will be damaged more likely in the lower frequency than in the higher frequency, while low-pass filtering affects higher frequency than lower ones. Layers or subbands with lower detector responses are discarded. This type of embedding combined with new detectors is more attack resilient to a possible erasure of the three subbands. At the embedding process [30], the image I, of size $2M \cdot 2N$, is decomposed into four levels using Daubechies-6 wavelet mother, where I_l^θ is the subband from level $l \in \{0,1,2,3\}$, and orientation $\theta \in \{0,1,2,3\}$ (corresponding to horizontal, diagonal and vertical detail subbands, and approximation subband). A binary watermark $x_l^\theta(i,j)$ is embedded in all coefficients from the subbands from level l by addition:

$$\tilde{I}_l^\theta(i,j) = I_l^\theta(i,j) + \alpha w_l^\theta(i,j)\, x_l^\theta(i,j), \tag{6}$$

where α is the embedding strength and $w_l^\theta(i,j)$ is a weighting function. The mask (or equivalently the weighting function) is built pixel by pixel, and it gives the maximum amount of modifications that can be applied to the corresponding DWT coefficient in the detail band without compromising watermark invisibility. This weighting function is a half of the quantization step. The quantization step of each coefficient is computed in [30] as the weighted product of three factors:

$$q_l^\theta(i,j) = \Theta(l,\theta)\,\Lambda(l,i,j)\,\Xi(l,i,j)^{0.2}, \tag{7}$$

and the embedding takes place only in the first level of decomposition, for $l = 0$. The first factor is the sensitivity to noise depending on the orientation and on the level of detail:

$$\Theta(l,\theta) = \begin{Bmatrix} \sqrt{2}, & \theta = 1 \\ 1, & \text{otherwise} \end{Bmatrix} \cdot \begin{Bmatrix} 1.00 & l = 0 \\ 0.32 & l = 1 \\ 0.16 & l = 2 \\ 0.10 & l = 3 \end{Bmatrix} \tag{8}$$

The second factor takes into account the local brightness based on the gray level values of the low pass version of the image:

$$\Lambda(l,i,j) = 1 + L'(l,i,j), \tag{9}$$

where

$$L'(l,i,j) = \begin{cases} 1 - L(l,i,j), & L(l,i,j) < 0.5 \\ L(l,i,j), & \text{otherwise} \end{cases}, \tag{10}$$

and

$$L(l,i,j) = I_3^3\left(1+\left\lfloor i/2^{3-l}\right\rfloor, 1+\left\lfloor j/2^{3-l}\right\rfloor\right)\Big/256. \tag{11}$$

The integer part operator from the right hand side is used to modify the size of the image I_3^3 in accordance with the requirements of the previous decomposition levels. It produces an interpolation of the initial image by multiple repetitions of each row and column. The quality of this procedure degrades rapidly with the increasing of rows and columns number. The third factor is computed as follows:

$$\Xi(l,i,j) = \sum_{k=0}^{3-l} 16^{-k} \sum_{\theta=0}^{2} \sum_{x=0}^{1} \sum_{y=0}^{1} \left[I_{k+l}^{\theta}\left(y+i/2^k, x+j/2^k\right)\right]^2 \cdot \mathrm{Var}\left\{ I_3^3\left(1+y+i/2^{3-l}, 1+x+j/2^{3-l}\right)\right\}_{x,y=0,1} \tag{12}$$

and it gives a measure of texture activity in the neighborhood of the pixel. This term is composed by the product of two contributions; the first is the local mean square value of the DWT coefficients in all detail subbands, while the second is the local variance of the low-pass subband. Both these contributions are computed in a small 2 × 2 neighborhood corresponding to the location (*i*, *j*) of the pixel. The first contribution is the distance from the edges, whereas the second one the texture. This local variance estimation is not so precise, because it is computed with a low resolution. In [31], the second factor from Eq. (12) is replaced by the local standard deviation of the image, which has a higher resolution. This is compressed in the wavelet domain to have the same size as the subband where the watermark is to be inserted:

$$\Xi(l,i,j) = \sum_{k=0}^{3-l} 16^{-k} \sum_{\theta=0}^{2} \sum_{x=0}^{1} \sum_{y=0}^{1} \left[I_{k+l}^{\theta}\left(y+i/2^k, x+j/2^k\right)\right]^2 \cdot \mathrm{DWT}_l^3\left\{\mathrm{Std}(I)_{x,y=0,\ldots,7}\right\} \tag{13}$$

An alternative for the computation of the local mean square value of the DWT coefficients in all detail subbands is to use wavelet interpolation. The second difference between [30] and [31] is that the luminance mask is computed on the approximation image from level *l*, where the watermark is embedded. The DWT of the original image using *l* decomposition levels was computed and the approximation sub-image corresponding at level *l* was separated, obtaining the image I_l^3. Relation (11) was replaced in [31] by:

$$L(l,i,j) = I_l^3(i,j)\big/256 \tag{14}$$

Since both factors already described are more dependent on the resolution level in the method proposed in [31], the noise sensitivity function is also replaced by:

$$\Theta(l,\theta) = \left\{\begin{matrix}\sqrt{2}, & \theta = 1 \\ 1, & \text{otherwise}\end{matrix}\right\}\left\{\begin{matrix}1.00 & l \in \{0,1\} \\ 0.66 & l = 2\end{matrix}\right\} \tag{15}$$

In [30], detection is made using the correlation between the marked DWT coefficients and the watermarking sequence to be tested for presence, for level $l = 0$:

$$\rho(l) = 4^l \sum_{\theta=0}^{2} \sum_{i=0}^{M/2^l-1} \sum_{j=0}^{N/2^l-1} \tilde{I}_l^{\theta}(i,j) x_l^{\theta}(i,j) \Big/ (3MN) \tag{16}$$

The correlation is compared to a threshold $T_{\rho(l)}$, computed to grant a given probability of false positive detection, using the Neyman-Pearson criterion. For example, if $P_f \le 10^{-8}$, the threshold is $T_{\rho(1)} = 3.97\sqrt{\sigma_{\rho(1)}^2}$, with $\sigma_{\rho(1)}^2$ being the variance of the wavelet coefficients, if the image was watermarked with a code Y other than X:

$$\sigma_{\rho(l)}^2 \approx \left(4^l/(3MN)\right)^2 \sum_{\theta=0}^{2} \sum_{i=0}^{M/2^l-1} \sum_{j=0}^{N/2^l-1} \left(\tilde{I}_l^{\theta}(i,j)\right)^2. \tag{17}$$

In [31] was considered the ratio between the correlation $\rho(l)$ in Eq. (16) and the image dependent threshold $T_{\rho(l)}$, hence the detector was viewed as a nonlinear function with a fixed threshold. Three detectors are being used. The first detector evaluates the watermark's presence on all resolution levels:

$$d_1 = \rho_{d1} / T_{d1} \tag{18}$$

where the correlation ρ_{d1} is given by:

$$\rho_{d1} = \sum_{l=0}^{2} \sum_{\theta=0}^{2} \sum_{i=0}^{M/2^l-1} \sum_{j=0}^{N/2^l-1} \tilde{I}_l^{\theta}(i,j)\, x_l^{\theta}(i,j) \Bigg/ \left(3MN \sum_{l=0}^{2} 4^{-l} \right) \tag{19}$$

The threshold for $P_f \leq 10^{-8}$ is $T_{d1} = 3.97\sqrt{\sigma^2_{\rho d1}}$, with:

$$\sigma^2_{\rho d1} \approx \sum_{l=0}^{2} \sum_{\theta=0}^{2} \sum_{i=0}^{M/2^l-1} \sum_{j=0}^{N/2^l-1} \left(\tilde{I}_l^{\theta}(i,j) \right)^2 \Bigg/ \left(3MN \sum_{l=0}^{2} 4^{-l} \right)^2 \tag{20}$$

The second detector considers the responses from different levels, as $d(l)=\rho(l)/T\rho_{(l)}$, with $l \in \{0,1,2\}$, and discards the detector responses with lower values:

$$d_2 = \max_{l} \{ d(l) \} \tag{21}$$

The third detector considers the responses from different subbands and levels, as $d(l,\theta) = \rho(l,\theta)/T(l,\theta)$, with $l,\ \theta \in \{0,1,2\}$, and discards the detector responses with lower values:

$$d_3 = \max_{l,\theta} \{ d(l,\theta) \} \tag{22}$$

where $\rho(l,\theta)$ and $T(l,\theta)$ are the correlations and thresholds for each subband. For $P_f \leq 10^{-8}$, the threshold is $T(l,\theta) = 3.97\sqrt{\sigma^2_{\rho(l,\theta)}}$, with $\sigma^2_{\rho(l,\theta)}$ the variance of wavelet coefficients from the subband (l,θ):

$$\rho(l,\theta) = 4^l \sum_{i=0}^{M/2^l-1} \sum_{j=0}^{N/2^l-1} \tilde{I}_l^{\theta}(i,j) x_l^{\theta}(i,j) \Big/ (MN) \tag{23}$$

$$\sigma^2_{\rho(l,\theta)} \approx 16^l \sum_{i=0}^{M/2^l-1} \sum_{j=0}^{N/2^l-1} \left(\tilde{I}_l^{\theta}(i,j) \right)^2 \Big/ (MN)^2 \tag{24}$$

3.2 Perceptual watermarks embedded in the HWT domain

The aim of this paper is perceptual watermarking in the HWT domain. Adapting the strategy already described in the previous paragraph to the case of HWT, we have decided to use the first three wavelet decomposition levels. We have considered two different embedding strategies, first we have embedded the watermark into the coefficients z_{+r} and z_{-r}. In this case the relations already described in the previous paragraph were used independently for each of these two images. The same message was embedded in both images, using the mask from [31]. The difference is that the orientations or preferential directions are in this case: atan(1/2), π/4, atan(2) (respectively for θ = 0,1,2), for the image z_{+r} and -atan(1/2), -π/4, -atan(2), (θ=0,1,2) for the image z_{-r}. At the detection side, we consider the pair of images (z_{+r}, z_{-r}), thus having twice as much coefficients than the standard approach, and θ takes all the possible values, ±atan(1/2), ±π/4, ±atan(2). This watermarking method will be called in the following Method 1.

Second, to exploit the better shift invariance of the HWT, we have embedded the watermark in the absolute values of the HWT coefficients. We consider the complex coefficients z_+ (having as real part the coefficients z_{+r} and as imaginary part the coefficients z_{+i}) and z_- (having as real part the coefficients z_{-r} and as imaginary part the coefficients z_{-i}) and we compute their absolute values, representing the new images I_l^{θ} corresponding to (6). The new embedding procedure is described by:

$$|\tilde{z}_{\pm}|_l^{\theta}(i,j) = \left| |z_{\pm}|_l^{\theta}(i,j) + \alpha w_l^{\theta}(i,j) x_l^{\theta}(i,j) \right|, \tag{25}$$

The same formula is used for the construction of the weighting function, so the relations (7) and (8) are kept in the new algorithm. For the computation of the second factor involved in the computation of the weighting function, relations similar with (9) and (10) are used in the new algorithm. To avoid the disadvantages of the interpolator in (11) we have preferred once again the relation (14). For the computation of the last factor we have used a relation similar with (13), but this time the variable θ takes six different values (three positive – for z_+ and three negative – for z_-), corresponding to the preferential directions of the HWT detail sub-images. For the computation of the local variance of the low-pass subband we have used the wavelet compression, obtaining the factor $\mathrm{DWT}_l^3\{\mathrm{Std}(I)\}(i,j)$. For the computation of the local mean square value of the HWT coefficients in all detail subbands we have used in this case an iterative algorithm based on wavelet interpolation. This kind of interpolation supposes to start with an image with known size and to consider it like the approximation sub-image obtained using a given DWT computed applying only one iteration. The corresponding detail sub-images are constructed supposing that all their coefficients are zero; the corresponding inverse DWT is computed and the result is a new image, having two times more lines and columns than the initial one. So, to compute the first factor of $\Xi(l,i,j)$ we perform the following operations:

$$\begin{aligned} &\mathrm{Int\_sum}_{\pm}(l,i,j) = \sum_{\theta=0}^{2}\left\{\left(\left|z_{\pm}\right|_l^{\theta}(i,j)\right)^2 + \left(\left|z_{\pm}\right|_l^{\theta}(i+1,j)\right)^2 + \left(\left|z_{\pm}\right|_l^{\theta}(i,j+1)\right)^2 + \left(\left|z_{\pm}\right|_l^{\theta}(i+1,j+1)\right)^2\right\} \\ &\mathrm{Int\_sum}(l,i,j) = \mathrm{Int\_sum}_{+}(l,i,j) + \mathrm{Int\_sum}_{-}(l,i,j) \end{aligned} \tag{24}$$

for l decreasing from 2 to zero. If l=2, then:

$$\Xi(2,i,j) = \mathrm{Int\_sum}(2,i,j)\cdot \mathrm{DWT}_2^3\{\mathrm{Std}(I)\}(i,j) \tag{25}$$

If l=1, we perform the wavelet interpolation of the image $\Xi(2,i,j)$ obtaining the new image $\mathrm{Interp}\{\Xi(2,i,j)\}$ and next we compute:

$$\Xi(1,i,j) = \mathrm{Int\_sum}(2,i,j)\cdot \mathrm{DWT}_1^3\{\mathrm{Std}(I)\}(i,j) + \frac{1}{16}\mathrm{Interp}\{\Xi(2,i,j)\} \tag{26}$$

Finally, if l=0, we perform the wavelet interpolation of the images $\mathrm{Interp}\{\Xi(2,i,j)\}$ and $\Xi(1,i,j)$ obtaining the new images $\mathrm{Interp}\{\mathrm{Interp}\{\Xi(2,i,j)\}\}$ and $\mathrm{Interp}\{\Xi(1,i,j)\}$ and next we compute:

$$\Xi(0,i,j) = \mathrm{Int\_sum}(2,i,j)\cdot \mathrm{DWT}_0^3\{\mathrm{Std}(I)\}(i,j) + \frac{1}{16}\mathrm{Interp}\{\Xi(1,i,j)\} + \frac{1}{256}\mathrm{Interp}\{\mathrm{Interp}\{\Xi(2,i,j)\}\} \tag{27}$$

Concerning the detection, we have used similar relation with (19) and (20). Of course, this time we have six preferential directions. The correlation at the level l is given by:

$$\rho_l = \frac{4^l}{6MN}\sum_{\theta=0}^{2}\sum_{i=0}^{M-1}\sum_{j=0}^{N-1}\left(\left|\tilde{z}_{+}\right|_l^{\theta}(i,j) + \left|\tilde{z}_{-}\right|_l^{\theta}(i,j)\right)\cdot x_l^{\theta}(i,j) \tag{28}$$

and it is compared to the threshold $T_{\rho_l} = 3.97\sqrt{\sigma_{\rho_l}^2}$, computed for a probability of false alarm smaller than 10^{-8}, where $\sigma_{\rho_l}^2$ is the variance of absolute value of HWT coefficients at level l, if the image was watermarked with a code Y≠X:

$$\sigma_{\rho_l}^2 \approx \frac{(4^l)^2}{(6MN)^2}\sum_{\theta=0}^{2}\sum_{i=0}^{M-1}\sum_{j=0}^{N-1}\left(\left|\tilde{z}_{+}\right|_l^{\theta}(i,j) + \left|\tilde{z}_{-}\right|_l^{\theta}(i,j)\right)^2. \tag{29}$$

We consider the ratios between the correlations ρ_l in Eq. (28) and the image dependent thresholds $T\rho_l$, for the first two decomposition levels. If at least one of these ratios is superior to 1 then the watermark is detected with a probability of false alarm inferior to 10^{-8}. This watermarking method will be called in the following Method 2.

4. SIMULATION RESULTS

Some simulation results, obtained using the image Lena, of size 512x512, are reported in the following. For $\alpha = 1.5$, and a watermark inserted in all levels: 0, 1 and 2, the image watermarked with method 1 has a peak signal-to-noise ratio (PSNR) of 35.63 dB. The original image, the corresponding watermarked image and the difference image are presented in figure 4. We have exposed our watermarked images at some common attacks: JPEG compression with different quality factors (Q), shifting, median filtering with different window sizes M, resizing with different scale factors, cropping with different areas remaining, gamma correction with different values of γ, blurring with a specified point spread function (PSF) and perturbation with AWGN with different variances and we have studied the robustness of the watermarking methods 1 and 2. The PSF is specified with the aid of two parameters: length L and angle β. Resistance to unintentional attacks, for watermarked image Lena, method 1, can be compared to the results obtained using the watermarking methods reported in [30] and [31] analyzing table 1. In the simulation corresponding to the watermarking method proposed in [31], we use the same watermark strength, 1.5 and we embed the watermark in all three wavelet decomposition levels, resulting in a PSNR of 36.86 dB. For the simulation corresponding to the watermarking method proposed in [30], we use the watermark strength 0.2 and the embedding is made only in the first resolution level, resulting in a similar quality of the images (PSNR=36.39 dB). Special attention was paid to the shifting attack. First the watermarked image was circularly shifted with *li* lines and *co* columns, obtained the attacked image $\left(\tilde{I}_t\right)$. Supposing that the numbers *li* and *co* are known, the messages at level *l* are circularly shifted with $li/2^l$ lines and $co/2^l$ columns obtaining the new messages $\left(x_t\right)_l^\theta$. Next the watermark was detected using the image $\left(\tilde{I}\right)_t$ and the messages $\left(x_t\right)_l^\theta$. The values obtained for *li*=128 and *co*=128 are presented in table 1.

From the results, it is clear that embedding in the real parts of the HWT transform yields in a higher capacity at the same visual impact and robustness. In fact the results obtained for method 1 are slightly better than the results obtained with the methods described in [30] and [31] for JPEG compression, median filtering with window size M=3, resizing and gamma correction. For the other attacks the results obtained using method 1 are similar with the results of the watermarking methods based on DWT. The case of the shifting attack is very interesting. In this case the robustness of the watermarking method is given by two properties: the shift invariance degree of the WT used and the masking ability. All the methods compared in table 1 are very robust against the shifting attack. The values of the ratios between the correlations and the image dependent thresholds obtained before and after the shifting attack are equal for all the methods compared in table 1. So, the ability of masking seems to be more important than the shift invariance degree of the WT used for the conception of counter-measures against the shifting attack, when the numbers of lines and columns used for the attack are already known. Of course, the detection of these numbers must also be realized, for the implementation of a strategy against the shifting attack. Concerning the method 2, we have used the value $\alpha = 1$ and we have obtained for the watermarked image a PSNR of 34.43 dB. First we have tested the proposed watermarked image against the additive white Gaussian noise (AWGN) attack. White noise with known variance was added at the watermarked image and next the watermark embedded was detected. The results obtained are presented in table 2. On the first column is indicated the value of the AWGN variance used in the current experiment. On the second column are presented the corresponding PSNRs obtained after the attack. On the third column are indicated the values obtained for the ratios between ρ_0 and $T\rho_0$ and on the last column are given the values of the ratios of the correlation and threshold obtained at the second decomposition level. For variances superior to var_no=16, this attack is useless because it is easy to observe the degradation of an image with a PSNR inferior to 25 dB. Second we have tested the watermarking method 2 against a shifting attack. The corresponding simulation results are presented in table 3. We have applied the same simulation strategy like in the case of method 1. Next, the original image *I* was modified by circular shifts using the corresponding numbers of lines and columns, obtaining the image I_t and the new messages $\left(x_t\right)_l^\theta$. Applying the same watermarking technique to the image I_t but using this time the messages $\left(x_t\right)_l^\theta$ another watermarked image, $\left(\tilde{I}_t\right)$ is obtained. We have appreciated the similitude of the images $\left(\tilde{I}\right)_t$ and $\left(\tilde{I}_t\right)$ with the aid of their mean square error expressed using the PSNRt in table 3. These values are high enough, being in average with less than 1 dB smaller than

Fig. 4. Original and watermarked images with method 1, for $\alpha = 1.5$, PSNR=35.63 dB; Difference image, amplified 8 times.

Table 1. Comparison of robustness for different unintentional attacks. The first method proposed here, as well as the traditional approaches from [30] and [31] are compared.

Attacks vs. detector response	Method proposed in [31]			Barni's method [30]	Method 1 based on HWT		
	all levels	max level	max subband		all levels	max level	max subband
Before attack	21.57	39.12	33.60	**44.31**	24.78	43.18	26.30
JPEG, Q=50	5.45	6.76	5.02	6.22	6.25	**7.87**	4.85
JPEG, Q=25	3.02	3.67	2.60	3.03	3.23	**4.19**	2.62
JPEG, Q=20	2.55	3.08	2.09	2.38	2.72	**3.58**	2.33
Shift, *li*=128, *co*=128	21.57	39.12	33.59	**44.31**	24.78	43.18	26.30
Median filtering, M=3	4.29	4.58	4.87	1.57	4.59	**5.42**	4.37
Median filtering, M=5	**1.66**	1.24	2.27	0.59	1.61	1.64	1.49
Resizing, 0.75	9.53	15.86	15.64	14.09	10.93	**19.34**	14.67
Resizing, 0.50	4.21	5.72	5.75	2.31	4.56	6.14	**8.71**
Cropping, 256x256	7.40	12.14	17.10	**18.08**	8.68	15.20	13.82
Cropping, 128x128	3.11	4.66	**8.31**	8.01	3.53	6.04	6.86
Cropping, 64x64	1.10	1.72	**4.45**	3.92	1.32	2.47	3.71
Gamma correction, γ=1.5	22.18	39.76	33.74	43.04	25.31	**43.61**	26.45
Gamma correction, γ=2	22.59	39.70	32.98	42.43	25.62	**43.24**	25.88
Blur, L=31, β=11	2.69	7.81	**9.56**	9.05	3.05	9.18	7.55

the PSNR of the image $\tilde{I}$. So, the shift invariance of the absolute values of the HWT coefficients is very good, and the watermark can be detected despite this attack for a large variety of lines and columns numbers. Comparing the detection ratios obtained using the proposed watermarking methods based on the HWT presented in table 1 (method 1) and in the

Table 2. The robustness of Method 2 against the AWGN attack.

var_no =1	PSNRa =34.24	rat1 =13.6	rat2=3.4
var_no =4	PSNRa =32.17	rat1 =10.9	rat2 =3.1
var_no = 9	PSNRa =27.96	rat1 =7	rat2=2.6
var_no =16	PSNRa =23.68	rat1 =4.3	rat2 =2.1
var_no =25	PSNRa =20.03	rat1 =3.4	rat2 =1.8
var_no =100	PSNRa =8.14	rat1 =2.4	rat2 =1.2

Table 3. The robustness of Method 2 against shifting.

li=16	*co*=16	PSNRt =33.82	rat1 =1.25
li =20	*co* =20	PSNRt =33.84	rat1 =1.51
li =24	*co* =24	PSNRt =33.78	rat1 =1.78
li =28	*co* =24	PSNRt =33.82	rat1 =1.65
li =32	*co* =32	PSNRt =33.77	rat1 =1.27

tables 2 and 3 (method 2), it can be observed that the detection results associated to method 1 are better than the corresponding results associated to method 2. A possible explanation for this behavior is based on the statistical analysis of wavelet coefficients. The methods described in [30] and [31] are based on the statistics of DWT coefficients. Practically, method 1 supposes the embedding into the coefficients of two DWTs, z_{+r} and z_{-r}, distributed following the same statistical model like the wavelet coefficients used in the methods described in [30] and [31]. In the case of method 2, the embedding is made in the coefficients $|z_+|$ and $|z_-|$ which are distributed following a different statistical model.

5. CONCLUSION

The HWT is a very modern WT as it has been formalized only two years ago. In this paper we have used a very simple implementation of this transform, which permits the exploitation of the mathematical results and of the algorithms previously obtained in the evolution of wavelets theory. It does not require the construction of any special wavelet filter. It has a very flexible structure, as we can use any orthogonal or bi-orthogonal real mother wavelets for the computation of the HWT. The proposed implementation leads to both a high degree of shift-invariance and to an enhanced directional selectivity in the 2D case. In the theoretical derivations reported in this paper we have considered an ideal Hilbert transformer.

We have proposed a new type of pixel-wise masking for robust image watermarking in the HWT domain. Modifications were made to two existing watermarking technique proposed in [30] and in [31], based on DWT. These techniques were selected for their good robustness against the usual attacks. The method proposed in [31] was inspired by the method proposed in [30], but it contains some modifications. The first modification is in computing the estimate of the variance, which gives a better measure of the texture activity. An improvement is also owed to the use of a better luminance mask. The third improvement proposed in [31] is to embed the watermark in the detail coefficients at all resolutions, except the coarsest level; this can be particularly useful against erasure of high frequency subbands containing the mark in the watermarking system proposed in [30]. A nonlinear detector with fixed threshold – as ratio between correlation and the image dependent threshold-has been conceived. Using it, three watermark detectors were proposed in [31]: 1) from all resolution levels, 2) separately, considering the maximum detector response for each level and 3) separately, considering the maximum detector response for each subband. Two HWT embedding mechanisms are proposed, the first one exploiting the coefficients z_{+r} and z_{-r}, and the second one the absolute values of the complex HWT coefficients z_+ and z_-. These mechanisms correspond to two new watermarking techniques called method 1 and method 2.

The simulation results presented in this paper illustrate the effectiveness of the proposed algorithms. We tested the robustness of our methods against different attacks, and found out that it is similar or better than the robustness of the methods described in [30] and [31] in the case of the image Lena.

Our watermarking methods have superior capacity than the method proposed in [30] and even [31].

Our research team will make a closer analysis on the effects of using realisable Hilbert transformers as the next step of HWT implementation development. We intend to enhance our simulation results in the future generalizing the comparison already made to the image database used in [31].

REFERENCES

[1] D. L. Donoho, I. M. Johnstone, "Ideal spatial adaptation by wavelet shrinkage", *Biometrika*, 81(3) : 425-455, 1994.

[2] N. Kingsbury, "Complex Wavelets for Shift Invariant Analysis and Filtering of Signals", *Applied and Comp. Harm. Anal.* 10, '01, 234-253.

[3] N. G. Kingsbury, "A Dual-Tree Complex Wavelet Transform with improved orthogonality and symmetry properties", *Proc. IEEE Conf. on Image Processing*, Vancouver, '00, paper 1429.

[4] A. Grossman and J. Morlet, "Decomposition of Hardy functions into square integrable wavelets of constant shape", *SIAM J. Math. Anal.*, vol. 15, '84, 723–736.

[5] I. W. Selesnick, R. G. Baraniuk, and N. G. Kingsbury, "The dual-tree complex wavelet transform", *IEEE Signal Processing Magazine*, vol. 22(6), '05, 123–151.

[6] N. Delprat, B. Escudié, P. Guillemain, R. Kronland-Martinet, Ph. Tchamitchian, and B. Torresani, "Asymptotic wavelet and Gabor analysis: Extraction of instantaneous frequencies", *IEEE Trans. Inform. Theory*, vol. 38, '92, 644–664.

[7] P. Auscher, "Il n'existe pas de bases d'ondelettes regulieres dans l'espace Hardy h²(\)", *C. R. Acad Sci Paris*, vol. 315, '92, 769–772.

[8] S. Barber and G. P. Nason, "Real nonparametric regression using complex wavelets", *J. Roy. Stat. Soc. B*, vol. 66, '04, 927–939.

[9] N. G. Kingsbury, "Image processing with complex wavelets", *Philosophical Transactions of the Royal Society of London A*, vol. 357, '99, 2543 – 2560.

[10] I. W. Selesnick, "The design of approximate Hilbert transform pairs of wavelet bases", *IEEE Trans. on Signal Processing*, vol. 50, '02, 1144–1152.

[11] I. W. Selesnick, "Hilbert transform pairs of wavelet bases", *IEEE Signal Processing Letters*, vol. 8, '01, 170–173.

[12] J.-M. Lina and M. Mayrand, "Complex daubechies wavelets", *Applied and Computational Harmonic Analysis*, vol. 2, '95, 219–229.

[13] S. Mallat, "A Wavelet Tour of Signal Processing", 2-nd Edition, *Academic Press*, New York, '99.

[14] S. C. Olhede, Georgios Metikas, "The Hyperanalytic Wavelet Transform", *Imperial College Statistics Section* Technical Report TR-06-02, May 23, '06.

[15] I. Adam, C. Nafornita, J-M Boucher, A. Isar, "A New Implementation of the Hyperanalytic Wavelet Transform", Proc. of IEEE Symposium *ISSCS 2007*, Iasi, Romania, '07, 401-404.

[16] G.P. Nason, "Choice of wavelet smoothness, primary resolution and threshold in wavelet shrinkage", *Statistics and Computing*, 12, '02, 219-227.

[17] M. Lang, H. Guo, J. E. Odegard, C. S. Burrus and R. O. Wells Jr., "Noise reduction using an undecimated discrete wavelet transform", *IEEE Signal Processing Lett.*, vol.3, no.1, '96, 10-12.

[18] R. Coifman and D. Donoho, "Translation invariant de-noising", Wavelets and Statistics, A. Antoniadis and G. Oppenheim Eds, Springer-Verlag, New York, '95, 125-150.

[19] P. Abry, "Transformées en ondelettes-Analyses multirésolution et signaux de pression en turbulence", Ph.D.dissertation, Université Claude Bernard, Lyon, France, '94.

[20] J. R. Higgins, "Bases for the Hilbert space of Paley-Wiener functions", Proc. *Aachener Colloquium*, '84, 274-278.

[21] A. Isar, "Nouvelles modalités de décomposition multiresolution des signaux à energie finie", *Quatorzième colloque GRETSI,* Juan-les-Pins, France, '93, 93-97.

[22] Felix C. A. Fernandes, Rutter L.C. van Spaendonck and C. Sindey Burrus "A New Framework for Complex Wavelet Transforms", *IEEE Trans. on Signal Processing*, vol. 51, no. 7, '00, 1825–1837.

[23] E. P. Simoncelli, W. T. Freeman, E. H. Adelson, D. J. Heeger, "Shiftable multi-scale transforms", *IEEE Trans. on Inform. Theory*, vol. 38, '92, 587 – 607.

[24] C. Davenport, "Commutative Hypercomplex Mathematics", http://home.usit.net/~cmdaven/cmdaven1.htm

[25] I. Adam, C. Nafornita, J.-M. Boucher and A. Isar, "A Bayesian Approach of Hyperanalytic Wavelet Transform Based Denoising", Proc. *IEEE International Conference WISP'07*, Alcala de Henares, Spain, '07, 237-242.

[26] Pierre Moulin and M. Kivanc Mihcak, "A Framework for Evaluating the Data-Hiding Capacity of Image Sources", *IEEE Trans. Image Processing*, 11(9), '02, 1029-1042.

[27] Li Hua and James E. Fowler, "A Performance Analysis of Spread-Spectrum Watermarking Based on Redundant Transforms", Proc. IEEE *Int. Conf. on Multimedia and Expo*, Lausanne, Switzerland, '02, vol. 2, 553–556.

[28] Patrick Loo, Nick Kingsbury, "Digital Watermarking Using Complex Wavelets", *ICIP 2000*.

[29] J. Daugman, "Two-dimensional spectral analysis of cortical receptive field profiles", *Vision Res.*, 20, '80, 847-856.

[30] M. Barni, F. Bartolini and A. Piva, "Improved wavelet-based watermarking through pixel-wise masking", *IEEE Trans. Image Processing*, 10, '01, 783-791.

[31] C. Nafornita, "A New Pixel-Wise Mask for Watermarking", Proc. *ACM Multimedia and Security MM&Sec*, Dallas, Sept '07, 221-228.

[32] D. Kundur, "Water-filling for Watermarking?" *Proc. IEEE Int. Conf. Multimedia and Expo*, NY, '00, 1287-1290.

[33] C. Podilchuk and W. Zeng, "Image-Adaptive Watermarking Using Visual Models", *IEEE Journal on Selected Areas in Communications*, 16, 4, May 1998, 525-539.

[34] C. Nafornita, C., A. Isar and M. Borda, "Image Watermarking Based on the Discrete Wavelet Transform Statistical Characteristics", Proc. *IEEE EUROCON 2005*, Serbia & Montenegro, 943-946.